**Full Title Page**

# Evaluation of Tumor-associated Stroma and its Relationship with Tumor Hypoxia using Dynamic Contrast-enhanced CT and $^{18}$F-Misonidazole PET in Murine Tumor Models

Sho Koyasu, MD, Yoshihisa Tsuji, MD, PhD, Hiroshi Harada, PhD, Yuji Nakamoto, MD, PhD, Tomomi Nobashi, MD, Hiroyuki Kimura, PhD, Kohei Sano, PhD, Koji Koizumi, RT, Masatsugu Hamaji, MD, and Kaori Togashi, MD, PhD,

From the Department of Diagnostic Imaging and Nuclear Medicine (S.K., Y.N., T.N., K.S., K.T.), Department of Gastroenterology and Hepatology (Y.T.), and Department of Radiation Oncology and Image-Applied Therapy (H.H.), Graduate School of Medicine, Division of Molecular Imaging, Radioisotope Research Center of Kyoto University (H.K), Clinical Radiology Service, Kyoto University Hospital (K.K.) and Department of Bioartificial Organs, Institute for Frontier Medical Science (M.H.), Kyoto University, Kyoto, Japan

**Corresponding author:** Yuji Nakamoto

Department of Diagnostic Imaging and Nuclear Medicine, Kyoto University Graduate School of Medicine, 54 Shogoin Kawahara-cho, Sakyo-ku, Kyoto 606-8507, Japan. Tel: +81-75-751-3760. Fax: +81-75-771-9709. Email: ynakamo1@kuhp.kyoto-u.ac.jp

**Funding information:** This study was funded by a Grant-in-Aid for JSPS Fellows from the Japan Society for the Promotion of Science (S.K.).

This work was presented by the first author (S.K.) at the IRIYA program in the RSNA 2014 meeting.

**Manuscript type:** Original Research

## (a) Advances in Knowledge

- The dynamic contrast-enhanced (DCE)-CT protocol described in our study enables measurement of the contrast in the interstitial space which is associated with the amount of stroma, as well as vascular flow velocity in murine tumor models (Pearson's correlation coefficient, R = 0.83; $P < 0.0001$); this method could be applied in clinical practice since the protocol requires the same scanner and contrast agent as those in clinical use.

- Tumor hypoxia was complementarily localized in tumor-associated stroma; $^{18}$F-fluoromisonidazole uptake was negatively correlated with the flow velocity as well as with the tumor-associated stroma (Pearson's correlation coefficient, R = -0.53; $P < 0.0001$; and R = -0.58; $P < 0.0001$, respectively).

## (b) Implication for Patient Care

The *in vivo* imaging approach for tumor-associated stroma using DCE-CT that we have developed may be translated into a clinical tool that could be used to monitor the effects of stroma-depleting drugs.

**(c) Summary Statement**

**Our method using DCE-CT can potentially be used to quantify the density of tumor-associated stroma; we found that tumor hypoxia was complementarily localized in tumor-associated stroma.**

**Abstract**

**Purpose:** To determine the relationship between the fractional interstitial volume (Fis) as calculated on dynamic contrast-enhanced computed tomography (DCE-CT) and tumor-associated stroma, and to analyze its spatial relationship with tumor hypoxia in several xenograft tumor models.

**Materials and Methods:** All animal experiments were approved by the Animal Research Committee of our institution. Mice with three different xenograft tumors (U251, CFPAC-1 and BxPC-3; n = 6, 8 and 6, respectively) underwent DCE-CT then hypoxia imaging using $^{18}$F-fluoromisonidazole positron emission tomography (FMISO-PET) within 24 hours. Immunohistochemical analysis for the detection of hypoxia markers, and to quantify microvascular and stromal density, was conducted using harvested tumors. We defined two DCE-CT parameters (amount of interstitial space which is associated with the amount of stroma [Fis] and flow velocity [Fv]) and quantitatively validated them using immunohistochemistry. The FMISO uptake within the tumor was also assessed in relation to DCE-CT parameters. Imaging and immunohistochemical parameters were assessed using the Kruskal-Wallis test, Wilcoxon rank-sum test and using Pearson's correlation coefficient.

**Results:** Almost no α-smooth muscle actin-positive cells were found in U251 xenograft, while abundant stroma was found in the entire BxPC-3 xenograft and in the periphery of the CFPAC-1 xenograft. Quantitative analysis demonstrated a significant correlation ($R = 0.83$; $P < 0.0001$) between Fis and stromal density. FMISO uptake had a negative correlation with Fis ($R = -0.58$; $P < 0.0001$), and with Fv ($R = -0.53$; $P < 0.0001$).

**Conclusion:** Our data show that DCE-CT can quantify parameters associated with tumor-associated stroma. Tumor hypoxia was complementarily localized in tumor-associated stroma in the models we assessed.

## Introduction

Tumor-associated stroma is a complex tissue comprising multiple cellular and non-cellular components, such as cancer-associated fibroblasts, pericytes, endothelial cells, lymphocytes, myeloid cells and extracellular matrix. Although these appear as benign components of tumors, they are considered as being able to promote tumor proliferation, invasion, metastases and resistance to therapy; they achieve this by creating a succession of the tumor microenvironments under the influence of cancer cells (1, 2). Accumulating evidence from clinical research has indicated tumor-associated stroma to be potential prognostic factors (3-7). For examples, larger amount of stroma is a strong prognostic variable in lung adenocarcinoma (5), gastric cancer (6), and triple negative breast cancer (7). Thus, there is a strong need for reliable biomarkers and non-invasive *in vivo* imaging strategies for the stromal components. However, to date, it has not been possible to use conventional imaging techniques to assess tumor stromal components in clinical practice, although considerable efforts have been devoted to developing novel imaging techniques (4, 8, 9).

Dynamic contrast-enhanced computed tomography (DCE-CT), also known as perfusion CT, is a technology used to quantify tissue hemodynamics in normal and pathologic tissues including cancers (10-12). We hypothesized that this technique has

potential in quantifying tumor-associated stroma using a double compartment model, where the first is vascular (plasma) compartment and the second is interstitial compartment (13). Although DCE-CT using this model has not yet been applied in the clinic, it would be easy to use it clinically because it only requires a CT scanner and an iodinated contrast agent. The phenomenon of delayed enhancement can explain the putative mechanism underlying the depiction of the stroma (14-16). The iodinated contrast agent cannot cross the intact cell membrane but can freely distribute in the interstitium of the tumor-associated stroma, where the volume for distribution increases because of fibrotic tissue and abundant extracellular matrix. There is also some evidence that this phenomenon of delayed-phase CT enhancement is prognostic (15).

In addition to the stromal components, hypoxia in malignant tumors is also a negative prognostic factor due to its association with aggressive phenotypes and therapeutic resistance. Tumor hypoxia is a condition where tumor cells have been deprived of sufficient oxygen and exist at distances of 70–100 μm from tumor blood vessels (17-19). There have been many studies involving imaging of *in vivo* hypoxia. Among them, $^{18}$F-fluoromisonidazole positron emission tomography (FMISO-PET) has been the most extensively studied so far (19, 20). Nevertheless, even FMISO-PET is still only available for research purposes.

Although not well elucidated, tumor-associated stroma and tumor hypoxia are reported to be related to each other in a “vicious” cycle that is amplified in a feed forward loop via the Hedgehog pathway, making tumors more aggressive and resistant to therapy (21, 22). Thus, an imaging technique for stromal components might enable analysis of the spatial relationship between tumor-associated stroma and tumor hypoxia *in vivo*, and evaluation of tumor hypoxia, albeit indirectly.

Our study aimed to determine the relationship between the fractional interstitial volume (Fis) as calculated on DCE-CT and tumor-associated stroma, and to analyze its spatial relationship with tumor hypoxia in several xenograft tumor models.

## Materials and Methods

### Experimental Overview

All animal experiments were approved by the Animal Research Committee of our institution. *In vivo* imaging (initially DCE-CT followed by FMISO-PET/CT within 24 hours) was performed in xenograft tumors with a maximum diameter of 6–10 mm. We investigated the association between DCE-CT parameters and tumor-associated stroma as compared with immunohistochemistry which was conducted on frozen sections of harvested tumors. The FMISO uptake within tumor was also compared to DCE-CT parameters and immunohistochemistry to evaluate the association between tumor hypoxia and tumor-associated stroma (Table 1).

### Tumor Cell Lines

Three cell lines (American Type Culture Collection, Manassas, VA, USA) were used, namely human pancreatic ductal adenocarcinomas (CFPAC-1 and BxPC-3) and human glioblastoma (U251). We considered BxPC-3 as a stroma-rich model because the BxPC-3 xenograft has previously been reported to have abundant stroma (23), whereas CFPAC-1 has moderate stroma and U251 has no stroma. These cell lines were maintained in Dulbecco's modified Eagle's medium with 10% fetal-bovine-serum and

1% penicillin-streptomycin.

The cells ($2\times10^6$/100-μL PBS) were subcutaneously inoculated into the backs of immunodeficient mice (ICR-nu/nu 8-week-old females; Charles River Laboratories International Inc., Frederick, MD, USA); these tumors were included in the same scan range as the left ventricle of mice, because arterial input function (AIF) obtained from time-density curve on the left ventricle is required for DCE-CT analysis. The maximum diameter of the tumor was measured. When the diameter reached between 6-10 mm, in vivo imaging was performed to the tumor. The number of tumor-bearing mice implanted with the CFPAC-1, BxPC-3 and U251 cell lines was six, eight and six, respectively.

**DCE-CT Imaging**

Animals were positioned prone and taped down on a half-round tube-shaped bed (26-mm diameter; NXMRTB21: Neomax Engineering, Osaka, Japan), and anesthetized by intraperitoneal administration of pentobarbital (65 mg/kg). Then, a 30 gauge needle (0.3 × 21 mm; Dentronics, Tokyo, Japan) connected to a polyethylene single-lumen tube (SP10: Natsume, Tokyo, Japan) was placed in the tail vein. Image acquisition was performed using a multi-detector CT (Aquilion 16: Toshiba Medical Systems, Otawara, Japan) with iodinated contrast agent (Iomeron 300: Eisai, Tokyo, Japan), which was

diluted to a concentration of 150 mgI/ml and administered at a dose of 750 mgI/kg with an injection rate of 150 μL/sec. Scanning tube voltage and tube current were 100 kVp and 30 mAs (60 mA; 0.5 s/rotation). Images were acquired for 300-second frame using a sequence of three consecutive scanner protocols. 1st period (0-50 seconds); A 50-second sequence of images was acquired every one second (0.5 pitch with 0.5 sec interval). Contrast agent was injected 4 seconds after the beginning of the scan (= 0 second). 2nd period (50-140 seconds); A 90-second sequence of images was acquired every 3 second. (0.5 pitch with 2.5 sec interval). 3rd period (140-300 seconds); A 160-second sequence of images was acquired every 8 second (0.5 pitch with 7.5 sec interval). These images were reconstructed into 1 mm × 16 slices without correction for beam hardening.

**$^{18}$F-FMISO-PET/CT Study**

The $^{18}$F-FMISO was synthesized as previously described (24) with slight modification (Appendix 1). The radiochemical purity of the $^{18}$F-FMISO produced was confirmed to be > 99%.

Animals were taped down on the same bed for DCE-CT and were imaged using a small-animal scanner (Triumph: TriFoil Imaging Inc., Chatsworth, CA, USA).

The animals were injected with FMISO (18.5 MBq) via the tail vein 2 hours before PET acquisition (30 min scan). CT scans were performed for anatomic reference (spatial resolution, 50 μm; 60 kV; 310 μA) after the PET study. During PET/CT, mice were anaesthetized using 2% isoflurane gas in an oxygen flow (2 L/min). PET images and CT images were reconstructed as follows: three-dimensional ordered-subset expectation maximization (5 min/frame) for PET; and a modified three-dimensional cone-beam Feldkamp algorithm resulting in a 0.177-mm iso-voxel with a 512 × 512 × 512 image volume for CT. Acquired PET and CT datasets were processed using PMOD Biomedical Image Quantification (PMOD Technologies Ltd., Zurich, Switzerland) software.

**Image Data Analysis**

DCE-CT analysis was performed using dedicated software (CT Perfusion Analysis, evaluation version: Ziosoft Inc., Tokyo, Japan). Two quantitative parameters were calculated: 1) Fv (1/100 min), calculated using a single compartment model (25) and 2) Fis (ml/100 ml), calculated using a double compartment model (13). The theoretical equations were defined by Cao et al., describing the time dependent flow of the solute into and out of the interstitial compartment, as represented by the bi-directional

trans-luminal permeability-surface area product (13). For analysis, in brief a time-density curve was obtained from changes in the CT values for each pixel (Fig E1 [online]). The ROIs placed on the left ventricle were used for AIF. Then, we calculated parameters which were displayed as color maps. The color map data were assessed by two board-certified radiologists (S.K. and T.N. with 5 and 6 years of experience, respectively) in consensus. To calculate Fv and Fis, the readers consensually placed square-shaped ROIs (as many locations as possible up to seven) measuring 1 $mm^2$ superimposed on each tumor devoid of necrotic area. We determined the necrotic area as follows: first we visually avoided of the very low Fv area, then we measured Fv value and confirmed that the Fv value of the ROI was more than 10.0 (1/100 min).

FMISO-PET/CT images were analyzed on a commercial workstation (Advantage Workstation 4.4: GE Healthcare, Fairfield, CT, USA). The data were assessed by the two readers in consensus. According to the ROIs on DCE-CT images, the readers placed a square-shaped ROI measuring 1 $mm^2$ superimposed at the same locations on each tumor; the readers were unaware of the results of DCE-CT parameters. The FMISO uptake parameter was defined as the SUVmax of each 1-$mm^2$ ROI on the tumor, divided by the mean uptake in muscle, which was considered as background uptake.

**Immunohistochemical Evaluation**

Immunohistochemical staining was performed on tissue sections at the maximum tumor diameter in the transaxial plane (Appendix 2). Microscopic images were acquired using a Biorevo BZ-9000 microscope (Keyence, Osaka, Japan). After visual landmarks such as tumor edges, shapes and skin were used for registration, square-shaped ROIs measuring 1 $mm^2$ were superimposed on each image involving α-smooth muscle actin (α-SMA) or CD31 staining, according to the ROIs on DCE-CT and FMISO-PET images evaluated by another reader unaware of the results regarding imaging parameters. The colors that α-SMA or CD31 were stained were separated using ImageJ software (with a plugin color deconvolution) to calculate the percentage of α-SMA or CD31 positive areas in each ROI, defined as “stromal density” or “microvascular density”, respectively.

**Statistical Analysis**

All imaging and immunohistochemical parameters were compared between three cell lines using the Kruskal-Wallis test and Wilcoxon rank-sum test with the Bonferroni correction. The relationship between Fis and stromal density was assessed using

Pearson’s correlation coefficient. The relationship between microvascular density and Fv was also assessed for validation of Fv. FMISO uptake and DCE-CT parameters and immunohistochemical parameters were reassessed using Pearson’s correlation coefficient. In our study, no gradations of correlation were defined because of its small sample size. A $P$ value < 0.05 was considered as being significant. Statistical analyses were performed using JMP Pro 11 (SAS Institute Inc., Cary, NC, USA) software.

## Results

### Lesion Characterization using Imaging and Immunohistochemistry

The DCE-CT parameters, FMISO uptake and immunohistochemical parameters were compared between the three tumor types. The mean diameters of the CFPAC-1, BxPC-3 and U251 tumors were 7.7, 8.3 and 7.8 mm, respectively. The imaging results regarding the tumors were as follows (Fig E2a-c [online]). For Fis, which targeted tumor-associated stroma, significant differences were observed in all pairs of the three tumors; BxPC-3 was the highest followed by CFPAC-1 and U251 (all $P < 0.01$). The differences in Fv which targeted flow velocity were also significant (BxPC-3 was the highest followed by CFPAC-1 and U251; all $P < 0.01$). For FMISO uptake, BxPC-3 was significantly lower than the other two tumor types (both $P < 0.0001$).

Regarding immunohistochemical parameters, almost no α-SMA-positive cells were detected in U251 tumors, while abundant stroma was revealed in the entire BxPC-3 tumor and moderate stroma in the periphery of CFPAC-1 tumor. The quantitative results regarding both stromal and microvascular density showed significant differences in all pairs of the three tumors (BxPC-3 was the highest, followed by CFPAC-1 and U251; all $P < 0.01$; Fig E2d-e [online]). In terms of histopathological structure, cancer cells without stroma that were located away from

CD31 positive cells or close to necrosis stained positively for pimonidazole, indicating that these cells were hypoxic. Representative examples of the images obtained using FMISO-PET/CT, DCE-CT and by immunohistochemistry for each tumor type are shown in Figs 1, 2 and Fig. E3 [online].

**Validation of Fis and Fv using Immunohistochemistry**

From quantitative analysis involving ROIs, a significantly correlation (R = 0.83; $P < 0.0001$) between Fis and the stromal density was shown (Fig 3). Because the distributions of each dot differed among the three tumor types, we also analyzed the correlation between Fis and stromal density for each tumor type separately, resulting that both CFPAC-1 and BxPC-3 tumors were correlated (R = 0.59; $P < 0.0001$; and R = 0.62; $P < 0.0001$, respectively). The U251 tumor did not show a correlation (R = 0.22; $P < 0.0001$) because most of the Fis values were distributed around zero. For vascular components, a significant correlation (R = 0.57; $P < 0.0001$) between Fv and microvascular density was found (Fig E4).

**Relationship between Tumor Hypoxia and Other Parameters**

We first analyzed the association between Fis and FMISO uptake, and found a negative

correlation (Fig 4). We also analyzed the association between stromal density and FMISO uptake, where the results also indicated a negative correlation ($R = -0.66$; $P < 0.0001$; Fig E5a), suggesting tumor-associated stroma complementarily localized to the tumor hypoxia. Then, to investigate the relationship between tumor hypoxia and the vascular component, because we assumed that the hypoxic areas were related to areas with lower vascular density and poorer perfusion, we compared FMISO uptake with the vascular components and found a negative correlation between FMISO uptake and Fv, which was considered to be a possible vascular perfusion marker ($R = -0.53$; $P < 0.0001$; Fig E5b). Additionally, there was a correlation between FMISO uptake and microvascular density ($R = -0.54$; $P < 0.0001$; Fig E5c). Using immunohistochemistry, we were able to observe the vascular endothelium colocalized within the tumor-associated stroma (Fig E6a and b), explaining why areas with high stromal density did not show tumor hypoxia. A positive correlation was found between stromal density and the vascular component (Fv and microvascular density, $R = 0.65$ and $R = 0.61$, respectively; Fig E6c and d).

## Discussion

In our study, a significant correlation was found between the imaging parameter (Fis), which targeted the contrast accumulation in the interstitial space and reflects tumor-associated stroma in this model, and stromal density quantified using immunohistochemistry; this finding supported our hypothesis that DCE-CT had the potential to depict a similar spatial distribution of tumor-associated stroma to that confirmed using histopathological analysis. Tumor-associated stroma is considered to be a potential target for new therapeutic agents and it has been reported that drugs that deplete the tumor-associated stroma, such as anti-Hedgehog pathway inhibitors (3, 26-29), might improve drug delivery and be effective in some malignancies. Thus, our method may have clinical utility in the evaluation and prediction of the response to new treatment approaches in future. In terms of the association between tumor hypoxia and tumor-associated stroma, FMISO uptake had a negative correlation with Fis and stromal density, as well as with vascular parameters. These results suggest that tumor hypoxia was complementarily localized to tumor-associated stroma and the vascular component.

Previously, some studies have reported on the imaging of tumor-associated stroma (9, 13, 22, 30, 31). Ko *et al.* described that apparent diffusion coefficient values were lower in the stroma poor group compared with the stroma-rich group in estrogen

receptor–positive breast cancer (4). There have also been studies that DCE-magnetic resonance imaging (DCE-MRI) techniques can characterize the stromal tissue outside the tumor (30); however, there has been some controversy. Ellingsen et al. reported the lack of a correlation between their imaging parameters and the stroma, and concluded that the potential of DCE-MRI was limited (31). Furthermore, in DCE-MRI, the concentration of gadolinium is considered not to be proportional to the detected signal changes (32), while it is assumed that the concentration of iodinated agent is proportional to the measured Hounsfield Unit in DCE-CT (33). Vandsburger et al. described an experimental study using ferritin heavy chain overexpressing fibroblasts detected using MRI, targeting cancer-associated fibroblasts (9), although the technique may not be adopted in clinical practice because it requires the genetic manipulation of a fibroblast (8), while our methods requires only iodinated contrast agent and CT scanner.

In our study, we observed that tumor-associated stroma was not always hypoxic, at least, as long as tumor-associated stroma contains vascular endothelium inside it. It has been reported that hypoxia and the stroma amplify each other *in vitro* (21), or that HIF-1α positive cells within tumor-associated stroma in pancreatic ductal adenocarcinoma caused the metastasis of pancreatic cancer (34). Lohse et al. reported

that tumor hypoxia strongly correlated with the stroma in some models, whereas it did not correlate with the stroma in one of their models (22), which is consistent with our results. We speculate that tumor hypoxia reflects many parameters in addition to tumor-associated stroma, such as oxygen supply in the vessels, the distance from the vessels, the interstitial pressure and the metabolic state of the tumor cells. Therefore, specific parameters such as Fv, Fis or FMISO uptake should be evaluated in case each parameter is crucial for predicting or monitoring the effect of certain drugs.

While our study demonstrated a promising method for estimating stromal density, certain limitations merit discussion. First, we compared tumors grown from three different cell lines. They could be good models for α-SMA positivity; however, other background factors differed. Second, we focused on α-SMA-positive cancer-associated fibroblasts as a marker (1), but α-SMA is not specific for tumor-associated stroma. Although we confirmed that the majority of CD31-positive cells were not vascular endothelium or pericytes by comparison with CD31-positive vascular components on the adjacent tissue sections, the color deconvolution methods may include non-specific cells. In addition, evaluation included extracellular matrix remains, which may be a false negative for α-SMA. Third, there were still other confounders which might increase the value of Fis in the following examples: necrosis,

edema in the interstitial space in inflammation, hemorrhage, and accumulations of amyloid or other substances which is normally unrelated to tumor-associated stroma. Our method may distinguish necrosis from stroma using Fv value, but to completely rule out the other factors, multimodal imaging combined with MR imaging or some other technique is desirable. Fourth, the tumor-associated stroma in the xenograft tumors may differ from that in humans. Solid cancers in human patients may contain a higher percentage of tumor-associated stroma than our tumor models. Finally, there is still room for improvement in the DCE-CT scanning protocol. Radiation exposure is a major concern regarding this modality. We have already reduced the number of scans relative to previous studies (13), but further studies to reduce the sampling rate without significantly affecting imaging potential are still necessary. Additionally, when applying our method into clinical practice in future, large motions such as respiration should be another concern because our models were well controlled by anesthesia. Thus, techniques such as noise reduction, or registration method for adjusting bulk motion, together with iterative reconstruction, may improve the image quality as well as the safety of our approach (35).

In conclusion, our method using DCE-CT can potentially be used to quantify the density of tumor-associated stroma; we found that tumor hypoxia was

complementarily localized in tumor-associated stroma.

**Practical Application**

Considering that contrast-enhanced CT is widely accessible, DCE-CT is a potentially translatable approach for objective quantification of tumor-associated stroma for future practical applications regarding monitoring the effects of stroma-depleting drugs.

## References


1. Pietras K, Ostman A. Hallmarks of cancer: interactions with the tumor stroma. Experimental cell research. 2010;316(8):1324-31.
2. Ryan DP, Hong TS, Bardeesy N. Pancreatic adenocarcinoma. N Engl J Med. 2014;371(11):1039-49.
3. Olive KP, Jacobetz MA, Davidson CJ, et al. Inhibition of Hedgehog signaling enhances delivery of chemotherapy in a mouse model of pancreatic cancer. Science. 2009;324(5933):1457-61.
4. Ko ES, Han BK, Kim RB, et al. Apparent Diffusion Coefficient in Estrogen Receptor-Positive Invasive Ductal Breast Carcinoma: Correlations with Tumor-Stroma Ratio. Radiology. 2014;271(1):30-7.
5. Maeshima AM, Niki T, Maeshima A, Yamada T, Kondo H, Matsuno Y. Modified scar grade: a prognostic indicator in small peripheral lung adenocarcinoma. Cancer. 2002;95(12):2546-54.
6. Wu Y, Grabsch H, Ivanova T, et al. Comprehensive genomic meta-analysis identifies intra-tumoural stroma as a predictor of survival in patients with gastric cancer. Gut. 2013;62(8):1100-11.
7. Moorman AM, Vink R, Heijmans HJ, van der Palen J, Kouwenhoven EA. The prognostic value of tumour-stroma ratio in triple-negative breast cancer. Eur J Surg Oncol. 2012;38(4):307-13.
8. Choyke PL. Science to Practice: imaging cancer-associated fibroblasts--no innocent bystanders. Radiology. 2013;268(3):617-8.
9. Vandsburger MH, Radoul M, Addadi Y, et al. Ovarian carcinoma: quantitative biexponential MR imaging relaxometry reveals the dynamic recruitment of ferritin-expressing fibroblasts to the angiogenic rim of tumors. Radiology. 2013;268(3):790-801.
10. Tsuji Y, Yamamoto H, Yazumi S, Watanabe Y, Matsueda K, Chiba T. Perfusion computerized tomography can predict pancreatic necrosis in early stages of severe acute pancreatitis. Clin Gastroenterol Hepatol. 2007;5(12):1484-92.
11. Ippolito D, Bonaffini PA, Ratti L, et al. Hepatocellular carcinoma treated with transarterial chemoembolization: dynamic perfusion-CT in the assessment of residual tumor. World J Gastroenterol. 2010;16(47):5993-6000.
12. Huellner MW, Pauli C, Mattei A, et al. Assessment of prostate cancer with dynamic contrast-enhanced computed tomography using an en bloc approach. Investigative radiology. 2014;49(9):571-8.

13. Cao M, Liang Y, Shen C, Miller KD, Stantz KM. Developing DCE-CT to quantify intra-tumor heterogeneity in breast tumors with differing angiogenic phenotype. IEEE Trans Med Imaging. 2009;28(6):861-71.
14. Saeed M, Hetts SW, Jablonowski R, Wilson MW. Magnetic resonance imaging and multi-detector computed tomography assessment of extracellular compartment in ischemic and non-ischemic myocardial pathologies. World journal of cardiology. 2014;6(11):1192-208.
15. Asayama Y, Yoshimitsu K, Irie H, et al. Delayed-phase dynamic CT enhancement as a prognostic factor for mass-forming intrahepatic cholangiocarcinoma. Radiology. 2006;238(1):150-5.
16. Lacomis JM, Baron RL, Oliver JH, 3rd, Nalesnik MA, Federle MP. Cholangiocarcinoma: delayed CT contrast enhancement patterns. Radiology. 1997;203(1):98-104.
17. Brown JM, Wilson WR. Exploiting tumour hypoxia in cancer treatment. Nat Rev Cancer. 2004;4(6):437-47.
18. Harada H. How can we overcome tumor hypoxia in radiation therapy? J Radiat Res. 2011;52(5):545-56.
19. Fleming IN, Manavaki R, Blower PJ, et al. Imaging tumour hypoxia with positron emission tomography. Br J Cancer. 2015;112(2):238-50.
20. Rasey JS, Grunbaum Z, Magee S, et al. Characterization of radiolabeled fluoromisonidazole as a probe for hypoxic cells. Radiat Res. 1987;111(2):292-304.
21. Spivak-Kroizman TR, Hostetter G, Posner R, et al. Hypoxia triggers Hedgehog-mediated tumor stromal interactions in pancreatic cancer. Cancer Res. 2013.
22. Lohse I, Lourenco C, Ibrahimov E, Pintilie M, Tsao MS, Hedley DW. Assessment of hypoxia in the stroma of patient-derived pancreatic tumor xenografts. Cancers. 2014;6(1):459-71.
23. Farace P, D'Ambrosio D, Merigo F, et al. Cancer-associated stroma affects FDG uptake in experimental carcinomas. Implications for FDG-PET delineation of radiotherapy target. Eur J Nucl Med Mol Imaging. 2009;36(4):616-23.
24. Oh SJ, Chi DY, Mosdzianowski C, et al. Fully automated synthesis of [18F]fluoromisonidazole using a conventional [18F]FDG module. Nuclear medicine and biology. 2005;32(8):899-905.
25. Sitek A, Sheiman RG. Small-bowel perfusion measurement: feasibility with single-compartment kinetic model applied to dynamic contrast-enhanced CT. Radiology. 2005;237(2):670-4.
26. Amakye D, Jagani Z, Dorsch M. Unraveling the therapeutic potential of the Hedgehog pathway in cancer. Nat Med. 2013;19(11):1410-22.

27. Rudin CM, Hann CL, Laterra J, et al. Treatment of medulloblastoma with hedgehog pathway inhibitor GDC-0449. N Engl J Med. 2009;361(12):1173-8.
28. Beatty GL, Chiorean EG, Fishman MP, et al. CD40 agonists alter tumor stroma and show efficacy against pancreatic carcinoma in mice and humans. Science. 2011;331(6024):1612-6.
29. Provenzano PP, Cuevas C, Chang AE, Goel VK, Von Hoff DD, Hingorani SR. Enzymatic targeting of the stroma ablates physical barriers to treatment of pancreatic ductal adenocarcinoma. Cancer cell. 2012;21(3):418-29.
30. Jones EF, Sinha SP, Newitt DC, et al. MRI enhancement in stromal tissue surrounding breast tumors: association with recurrence free survival following neoadjuvant chemotherapy. PloS one. 2013;8(5):e61969.
31. Ellingsen C, Egeland TA, Galappathi K, Rofstad EK. Dynamic contrast-enhanced magnetic resonance imaging of human cervical carcinoma xenografts: pharmacokinetic analysis and correlation to tumor histomorphology. Radiother Oncol. 2010;97(2):217-24.
32. Fieselmann A, Kowarschik M, Ganguly A, Hornegger J, Fahrig R. Deconvolution-Based CT and MR Brain Perfusion Measurement: Theoretical Model Revisited and Practical Implementation Details. International journal of biomedical imaging. 2011;2011:467563.
33. Miles KA, Young H, Chica SL, Esser PD. Quantitative contrast-enhanced computed tomography: is there a need for system calibration? Eur Radiol. 2007;17(4):919-26.
34. Ide T, Kitajima Y, Miyoshi A, et al. The hypoxic environment in tumor-stromal cells accelerates pancreatic cancer progression via the activation of paracrine hepatocyte growth factor/c-Met signaling. Ann Surg Oncol. 2007;14(9):2600-7.
35. Khawaja RD, Singh S, Blake M, et al. Ultra-low dose abdominal MDCT: Using a knowledge-based Iterative Model Reconstruction technique for substantial dose reduction in a prospective clinical study. Eur J Radiol. 2015;84(1):2-10.

**Table 1**

| Target | Name | Explanation | Modality | Definition and Unit |
|---|---|---|---|---|
| Hypoxia | FMISO uptake | Nitroimidazole derivates diffuse across cell membranes. Under hypoxic condition, they are reduced and bind selectively to macromolecules within the cells. | PET | SUVmax on tumor divided by mean muscle uptake (no unit) |
| | Pimonidazole | | IHC | - |
| Tumor-associated stroma | Fis | Imaging biomarker for the contrast in the interstitial space which is associated with the amount of tumor-associated stroma. | DCE-CT | (ml/100 ml) |
| | Stromal density | The area of α-SMA positive cells, which is a marker for cancer-associated fibroblasts. | IHC | The percentage of positive area (%) |
| Vascular components | Fv | Imaging biomarker for flow velocity of the artery. | DCE-CT | (1/100 min) |
| | Microvascular density | The area of CD31 positive cells which is a marker for the vascular endothelium. | IHC | The percentage of positive area (%) |

FMISO = fluoromisonidazole

IHC = immunohistochemistry

PET = positron emission tomography

DCE-CT = dynamic contrast-enhanced computed tomography

α-SMA: α-smooth muscle actin

**Figure Captions**

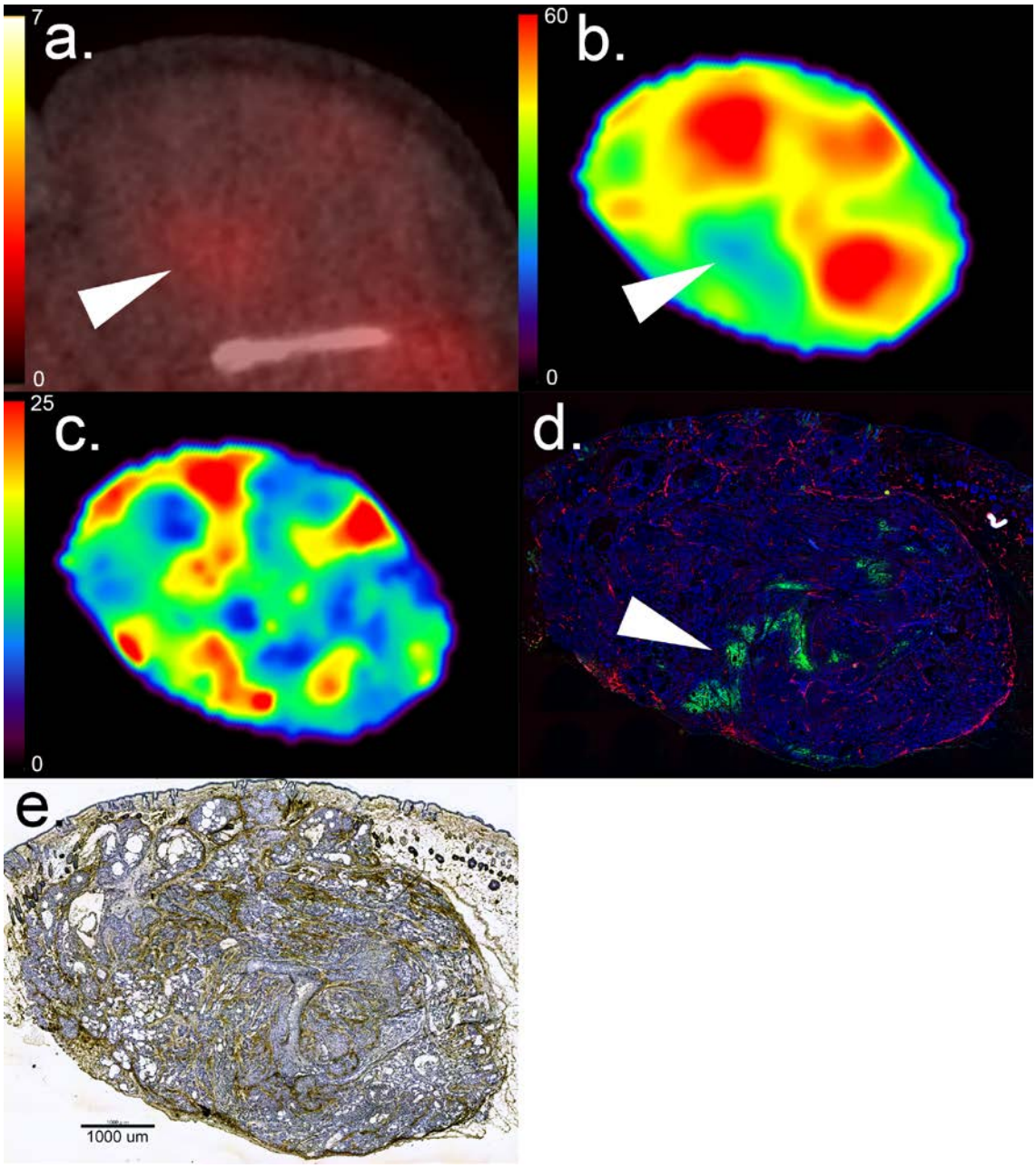


**Figure 1:** Representative image and immunohistochemistry of a BxPC-3 tumor (12-week-old female; 30.6 g). In BxPC-3 tumor, abundant stroma was revealed in the entire tumor by the color map of Fis and α-smooth muscle actin (SMA), which means this tumor was appropriate as a stroma-rich model. No clear necrotic area is shown in

any images or immunohistochemistry. 18F-fluoromisonidazole uptake has a focal distribution and pimonidazole is positive in almost the same location (arrowheads), which suggests there are not many hypoxic cells in BxPC-3 tumor. **(a)** $^{18}$F-fluoromisonidazole positron emission tomography/computed tomography. **(b)** Flow velocity (Fv) (1/100min) measured using dynamic contrast-enhanced computed tomography (DCE-CT). **(c)** Amount of tumor-associated stroma (Fis) (ml/100 ml) measured using DCE-CT. **(d)** Fluorescent staining for pimonidazole (green), CD31 (red) and Hoechst33342 (blue). **(e)** α-SMA detected using 3,3′-diaminobenzidine staining.

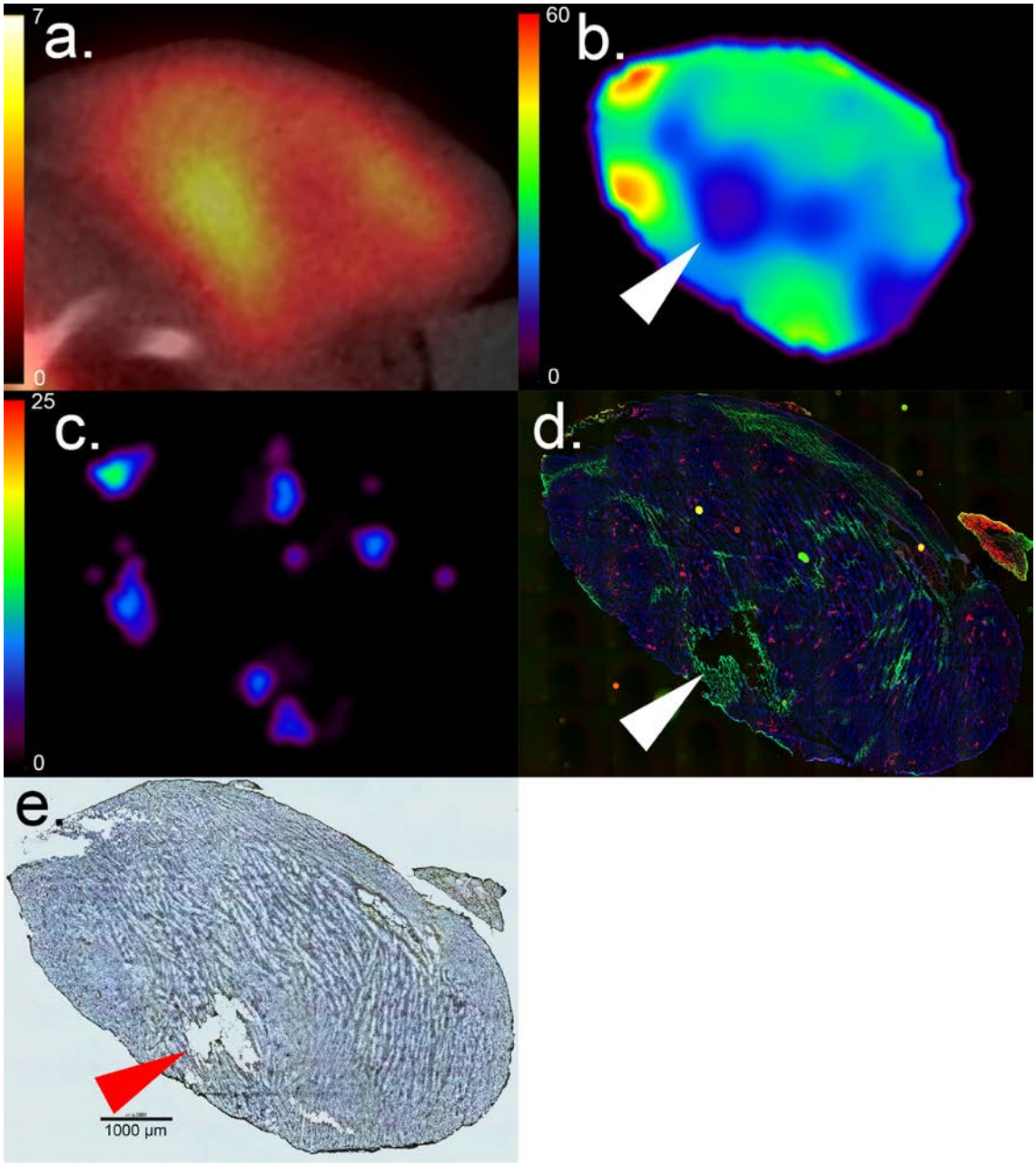


**Figure 2:** Representative image and immunohistochemistry of a U251 tumor (19-week-old female; 26.4 g). Almost no α-SMA-positive cells can be seen in the tumor, which means this tumor was appropriate as a stroma-scant model. The Fis is zero or very low in the entire tumor. Focal necrosis is shown where low Fv is depicted (arrowhead) and is surrounded by pimonidazole-positive cells. The hypoxic cells exist

approximately 100 μm from tumor blood vessels (CD31-positive cells). **(a)** $^{18}$F-fluoromisonidazole positron emission tomography /computed tomography. **(b)** Flow velocity (Fv) (1/100 min) measured using dynamic contrast-enhanced computed tomography (DCE-CT). **(c)** Amount of tumor-associated stroma (Fis) (ml/100 ml) measured using DCE-CT. **(d)** Fluorescent staining for pimonidazole (green), CD31 (red) and Hoechst33342 (blue). **(e)** α-smooth muscle actin (α-SMA) detected using 3,3′-diaminobenzidine staining.

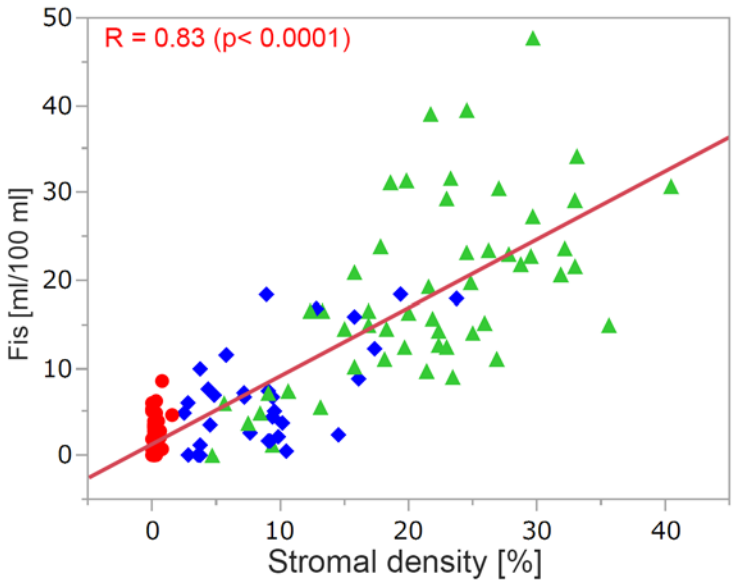


**Figure 3:** Histological validation of the amount of tumor-associated stroma (Fis). The graph shows a correlation between Fis and stromal density is shown (R = 0.83; *P* < 0.0001). Red circular-shaped points, blue diamond-shaped points, and green triangular shaped points represent U251, CFPAC-1, and BxPC-3, respectively.

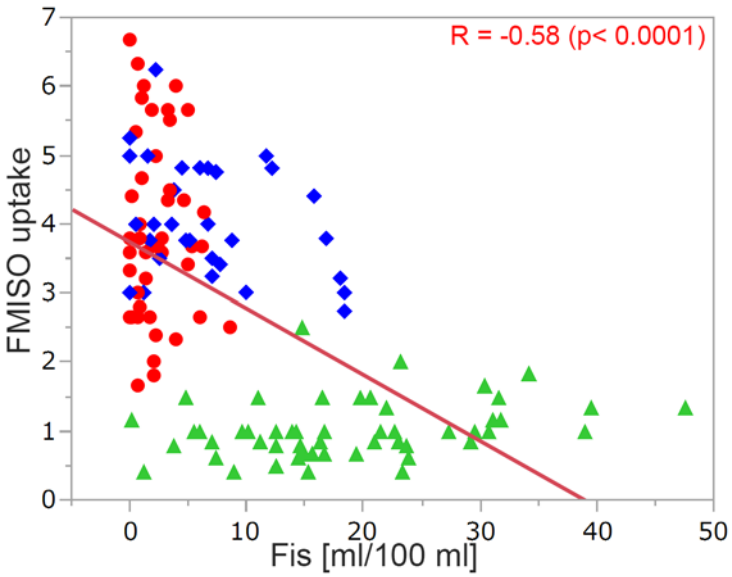


**Figure 4:** Relationship between tumor hypoxia and tumor-associated stroma. A negative correlation between $^{18}$F-fluoromisonidazole (FMISO) uptake and the amount of tumor-associated stroma (Fis) was revealed ($R = -0.58$; $P < 0.0001$). Red circular-shaped points, blue diamond-shaped points, and green triangular shaped points represent U251, CFPAC-1, and BxPC-3, respectively.

**Appendix 1**

**Synthesis of $^{18}$F-FMISO**

1-(2′-nitro-1′-imidazolyl-2-O-tetrahydropyranyl-3-O-toluenesulphonylpropanediol (NITTP; 5 mg) was added to the reaction vessel containing the $^{18}$F and Kryptofix222 in anhydrous acetonitrile (0.3 ml), and the mixture was heated at 110°C for 10 min. After cooling, 2N HCl was added to the resulting mixture, followed by heating at 80°C for 2 min. After neutralizing with 2N NaOH, $^{18}$F-FMISO was purified using an HPLC system with a reversed phase C-18 column (XBridge 5C18, 10 × 250 mm: Waters, Milford, MA, USA). The mobile phase used was $H_2O$/EtOH (97/3 v/v) at a flow rate of 5 ml/min. The radiochemical purity of the $^{18}$F-FMISO produced was determined using HPLC under the same conditions mentioned above. The radiochemical purity was > 99 %.

**Appendix 2**

**Immunohistochemical Staining Protocols**

Xenograft tumors were surgically excised at 90 min after an intraperitoneal injection of 60-mg/kg pimonidazole hydrochloride (Natural Pharmacia International Inc., Burlington, MA, USA). Frozen sections (6-μm thick) of the xenografts were prepared with OCT compound (Sakura Finetek, Tokyo, Japan) and a cryostat microtome (CM3050S: Leica, Solms, Germany). Fluorescent immunostaining was performed using Hoechst 33342 (Life Technologies, Carlsbad, CA, USA; 1 mg/ml solution), rat anti-mouse CD31 antibody (dilution of 1:2000: BD Biosciences, San Jose, CA, USA), and FITC-conjugated anti-pimonidazole mouse monoclonal antibody (dilution of 1:1000; Hypoxyprobe-1: Natural Pharmacia International Inc., Burlington, MA, USA): nuclear counterstain; vascular endothelium; and hypoxic cells, respectively. CD31 was detected using Alexa Fluor 594 goat anti-rat IgG (dilution of 1:2000; Life Technologies, Carlsbad, CA, USA). On the adjacent tissue section to that used for fluorescent immunohistochemistry, we performed anti-α-SMA staining as a marker for tumor-associated stroma, using mouse monoclonal antibody (dilution of 1:300; Sigma-Aldrich, St. Louis, MO, USA). α-SMA was detected using avidin-biotin-peroxidase complex (ABC-Elite: Vector Laboratories, Burlingame, CA,

USA) at a dilution of 1:100 in BSA and the nuclei were counterstained with hematoxylin.

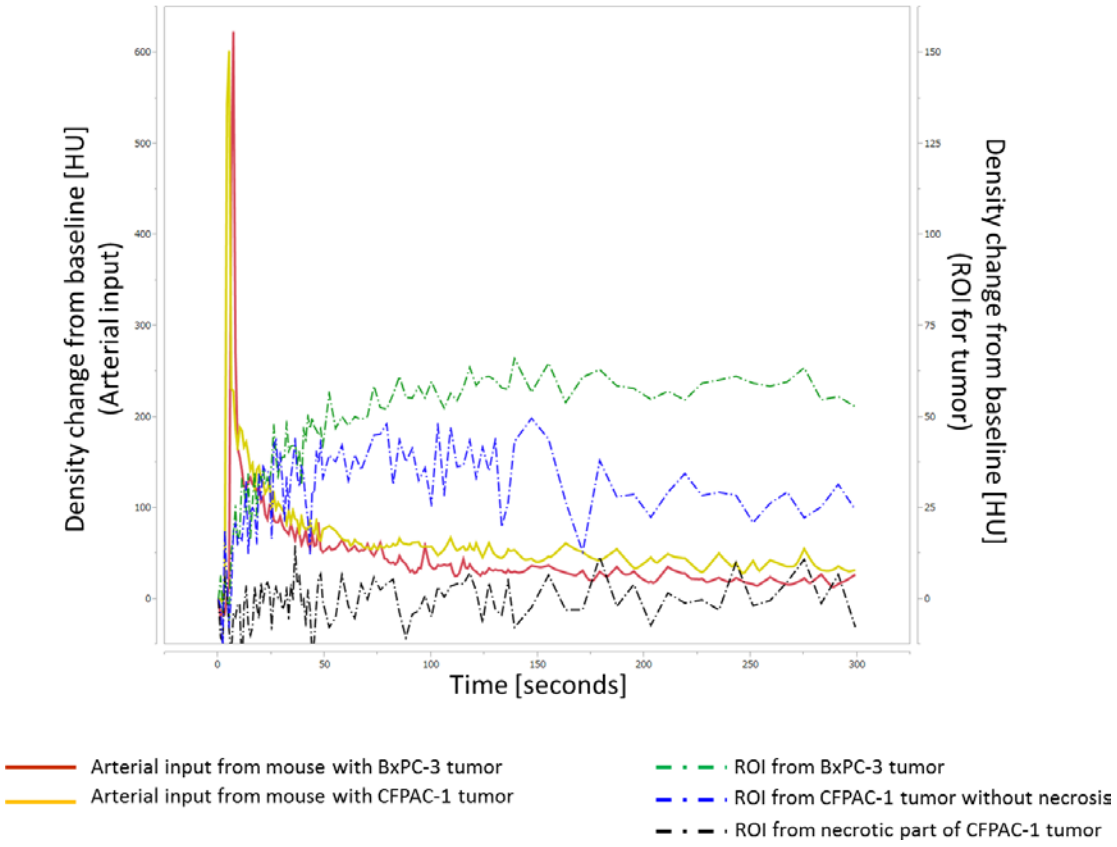


**Figure E1:** Representative time-density curves (TDC) for arterial input function (AIF) and region of interest (ROI) from the tumor. Each TDC for arterial input has an intense and narrow peak. The TDC for the ROI regarding the BxPC-3 tumor, which has abundant stroma, shows retention of contrast agent in the late phase (green dot-dash line), while that regarding the CFPAC-1 tumor without necrosis shows a slight decrease from the peak (blue dot-dash line). The TDC for the necrotic region shows almost no change (black dot-dash line). The left scale bar is for AIFs and the right scale bar is for ROIs for the tumors. HU, Hounsfield units.

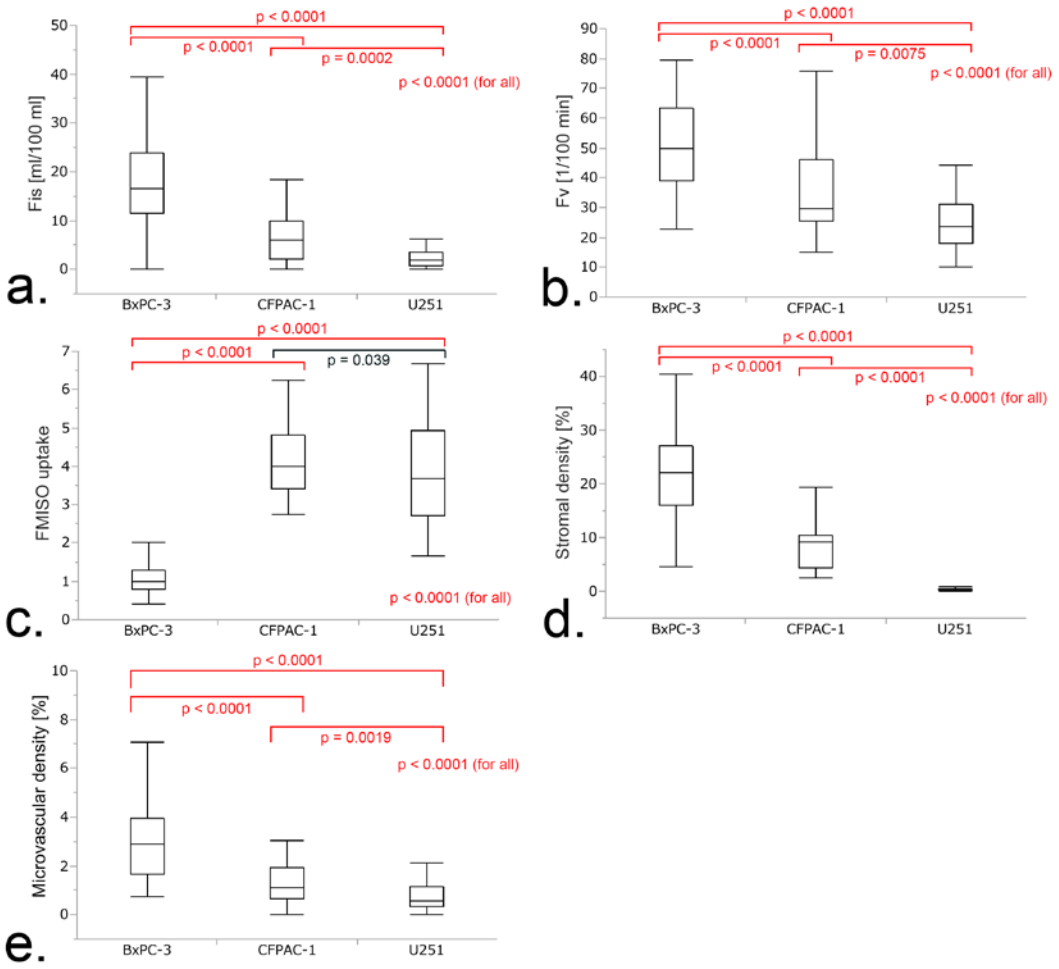


**Figure E2:** Kruskal-Wallis test and Wilcoxon rank-sum test used for comparing the imaging and immunohistochemical parameters between three groups. The significance level was adjusted using the Bonferroni correction (0.05/3 = 0.0167) for the multiple pair-wise comparisons. Both the amount of tumor-associated stroma (Fis) and flow velocity (Fv) values were significantly different between the three groups **(a)** and **(b)**. For $^{18}$F-fluoromisonidazole uptake, BxPC-3 was significantly lower than the other two cell lines **(c)**. Both stromal density and microvascular density were also significantly different between the three groups **(d)** and **(e)**.

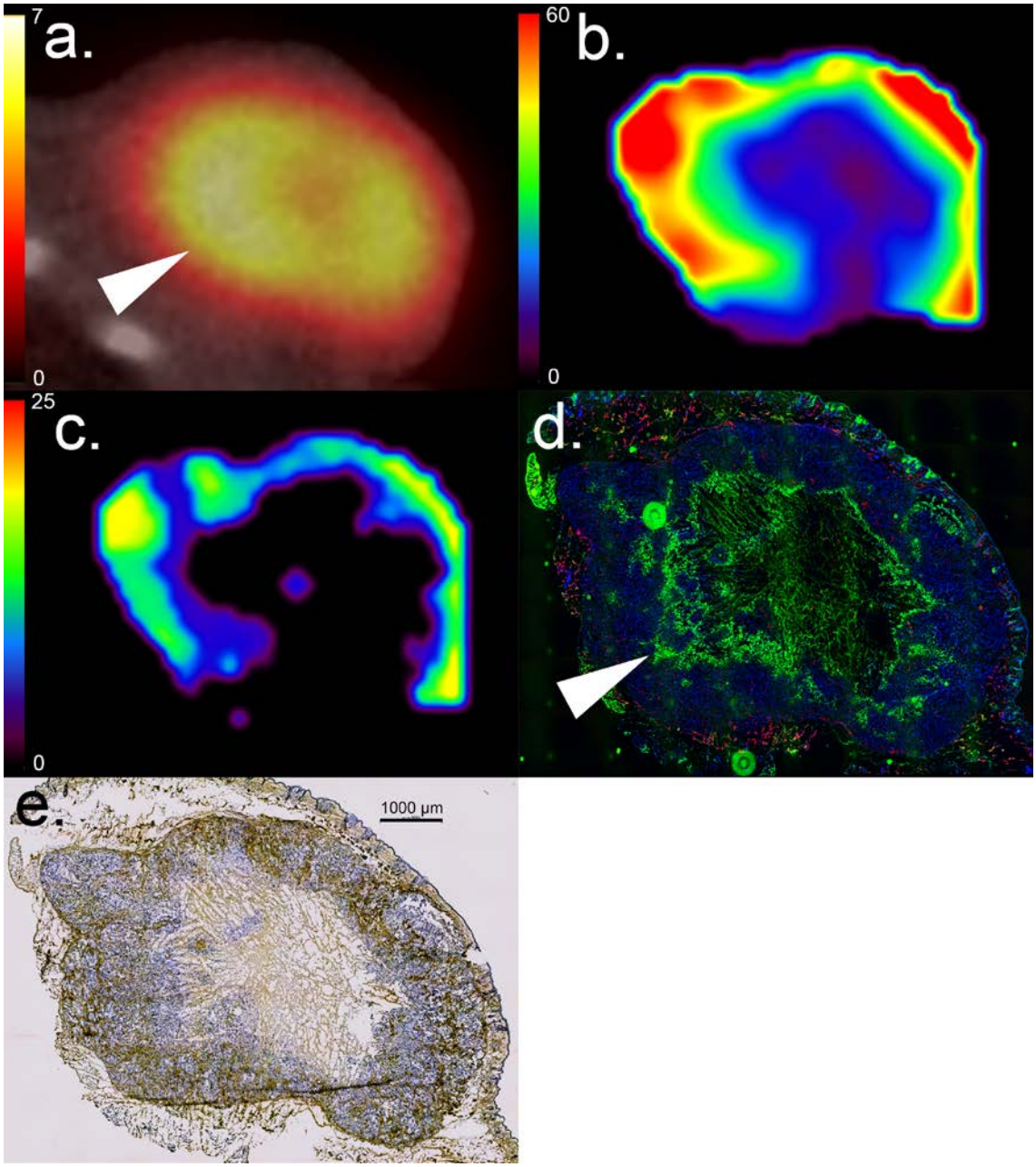


**Figure E3:** Representative image and immunohistochemistry of a CFPAC-1 tumor (12-week-old female; 30.0 g). Almost no α-SMA-positive cells can be seen in the tumor, which means this tumor was appropriate as a stroma-scant model. The Fis is zero or very low in the entire tumor. Focal necrosis is shown where low Fv is depicted (arrowhead) and is surrounded by pimonidazole-positive cells. The hypoxic cells exist

approximately 100 μm from tumor blood vessels (CD31-positive cells). **(a)** $^{18}$F-fluoromisonidazole positron emission tomography /computed tomography. **(b)** Flow velocity (Fv) (1/100 min) measured using dynamic contrast-enhanced computed tomography (DCE-CT). **(c)** Amount of tumor-associated stroma (Fis) (ml/100 ml) measured using DCE-CT. **(d)** Fluorescent staining for pimonidazole (green), CD31 (red) and Hoechst33342 (blue). **(e)** α-smooth muscle actin (α-SMA) detected using 3,3′-diaminobenzidine staining.

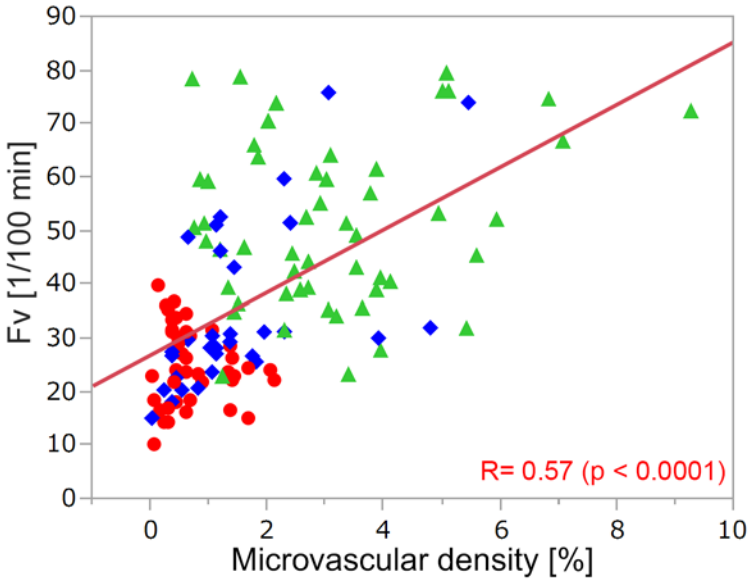


**Figure E4:** Histological validation of the relationship between Fv and microvascular density, where there is a correlation between Fv and microvascular density is shown (R = 0.57; P < 0.0001).

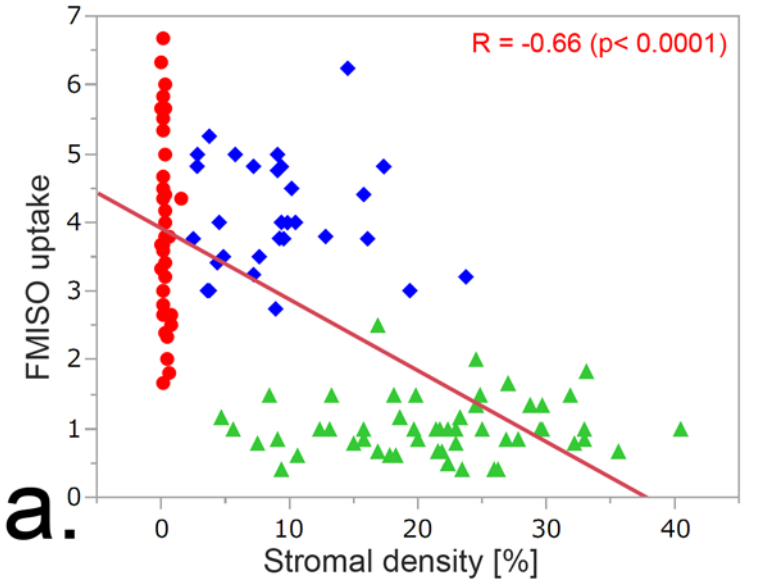
R = -0.66 (p< 0.0001)
FMISO uptake
Stromal density [%]
a.

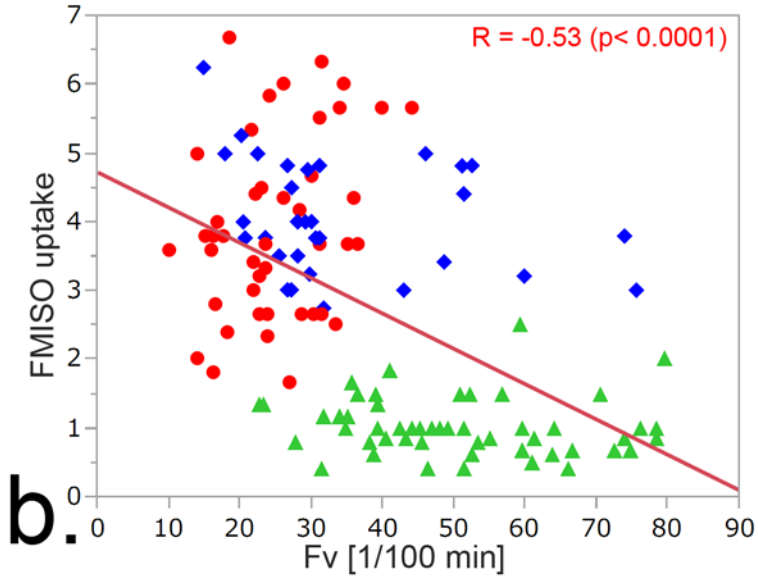
R = -0.53 (p< 0.0001)
FMISO uptake
Fv [1/100 min]
b.

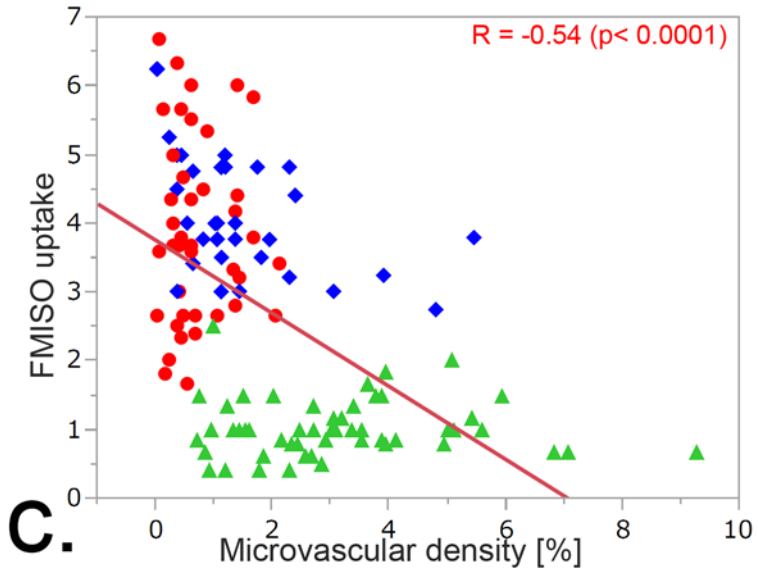
R = -0.54 (p< 0.0001)
FMISO uptake
Microvascular density [%]
c.

**Figure E5: (a)** A negative correlation between stromal density and $^{18}$F-fluoromisonidazole (FMISO) uptake (R = −0.66, $P < 0.0001$); **(b)** A negative correlation between Fv and FMISO (R = −0.53; $P < 0.0001$); **(c)** A negative correlation between microvascular density and FMISO (R = −0.54; $P < 0.0001$);

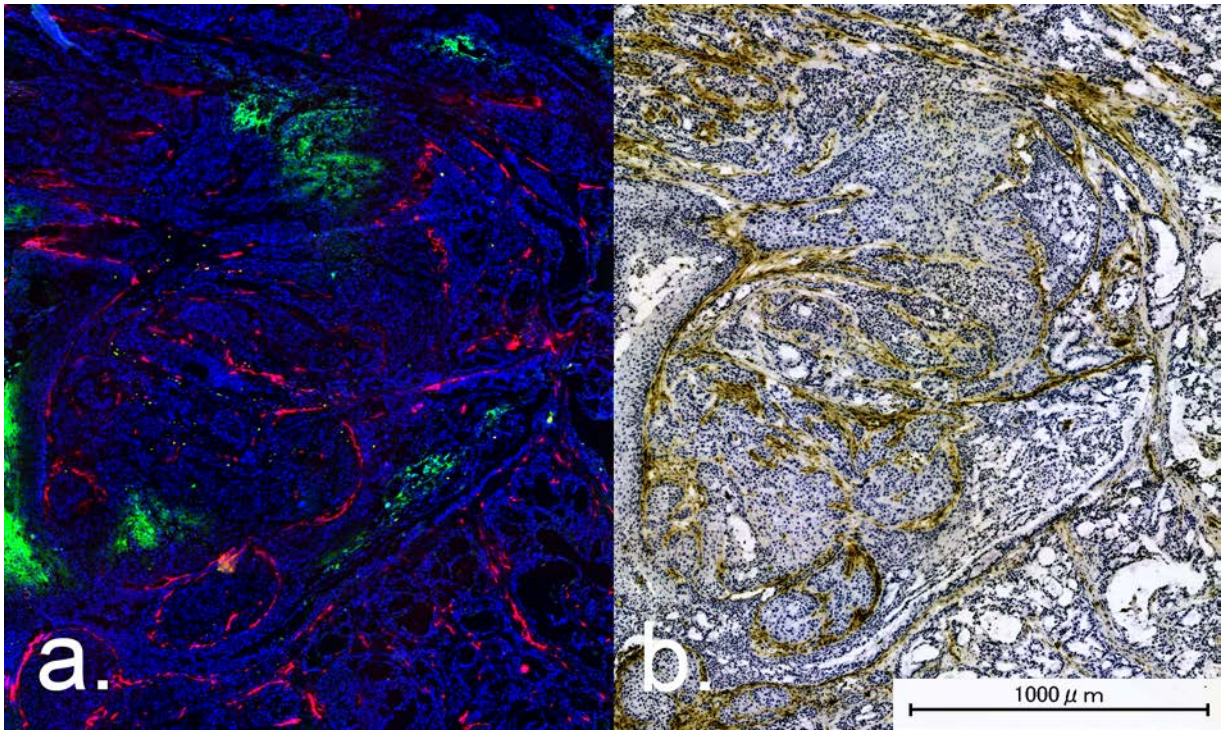
a.
b.
1000 μ m

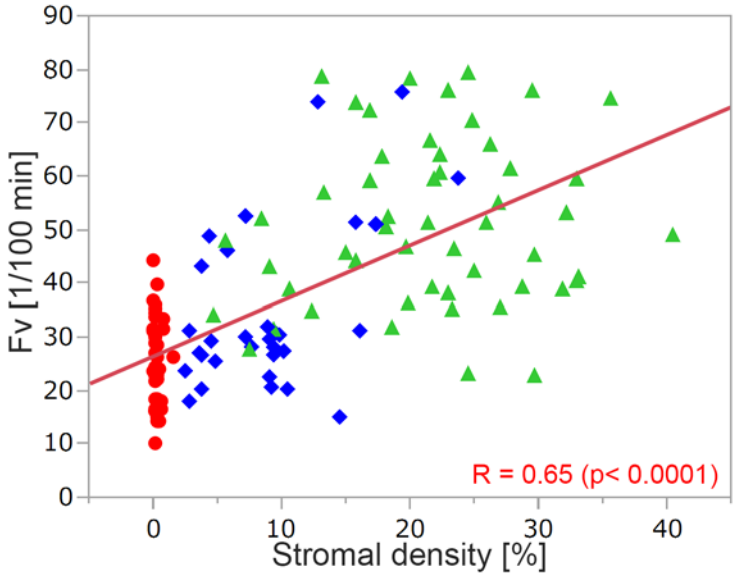
Fv [1/100 min]
Stromal density [%]
R = 0.65 (p< 0.0001)
0
10
20
30
40
50
60
70
80
90
0
10
20
30
40

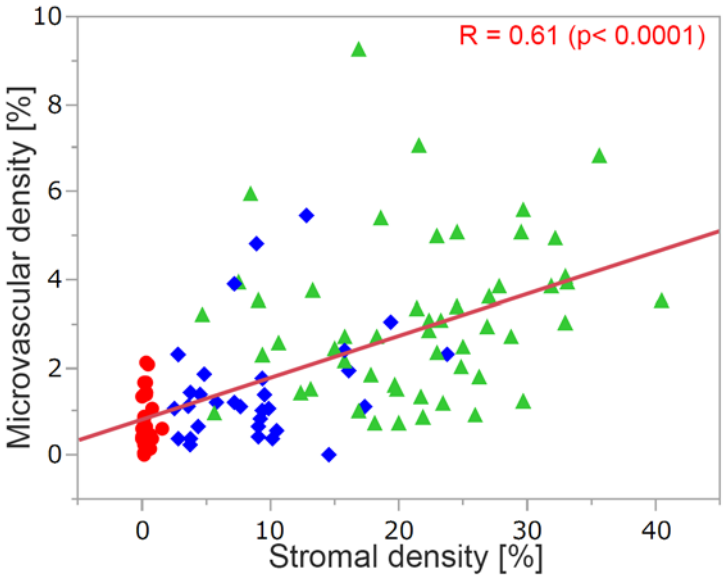


**Figure E6:** Relationship between tumor hypoxia and tumor-associated stroma, and vascular parameters. **(a)** Fluorescent staining for pimonidazole (green), CD31 (red) and Hoechst33342 (blue). **(b)** α-smooth muscle actin detected using 3,3′-diaminobenzidine staining, where the vascular endothelium is colocalized within the tumor-associated stroma. **(c, d)** A positive correlation (R = 0.65; $P < 0.0001$) is shown between stromal density and the vascular component.